ACS APPLIED MATERIALS & INTERFACES

Research Article

www.acsami.org

Synthesis of Uniform CdS Nanospheres/Graphene Hybrid Nanocomposites and Their Application as Visible Light Photocatalyst for Selective Reduction of Nitro Organics in Water

Zhang Chen, Siqi Liu, Min-Quan Yang, and Yi-Jun Xu*

State Key Laboratory Breeding Base of Photocatalysis, College of Chemistry and Chemical Engineering, Fuzhou University, Fuzhou 350002, People's Republic of China

Supporting Information

ABSTRACT: We report the self-assembly of uniform CdS nanospheres/graphene (CdS NSPs/GR) hybrid nanocomposites via electrostatic interaction of positively charged CdS nanospheres (CdS NSPs) with negatively charged graphene oxide (GO), followed by GO reduction via a hydrothermal treatment. During this facile two-step wet chemistry process, reduced graphene oxide (RGO, also called GR) and the intimate interfacial contact between CdS NSPs and the GR sheets are achieved. Importantly, the CdS NSPs/GR nanocomposites exhibit a much higher photocatalytic performance than bare CdS NSPs toward selective reduction of nitro organics to corresponding amino organics under visible light irradiation. The superior photocatalytic performance of the CdS NSPs/GR nanocomposites can be attributed to the intimate interfacial contact between CdS NSPs and the GR sheets, which would maximize the excellent electron conductivity and mobility of GR that in turn markedly contributes to improving the fate and transfer of photogenerated charge carriers from CdS NSPs under visible light irradiation. Moreover, the photocorrosion of CdS and the photodegradation of GR can be efficiently inhibited. The excellent reusability of the CdS NSPs/GR nanocomposites can be attributed to the synergetic effect of the introduction of GR into the matrix of CdS NSPs and the addition of ammonium formate as quencher for photogenerated holes. It is hoped that our current work could promote us to efficiently harness such a simple and efficient self-assembly strategy to synthesize GR-based semiconductor composites with controlled morphology and, more significantly, widen the application of CdS/GR nanocomposite photocatalysts and offer new inroads into exploration and utilization of GR-based semiconductor nanocomposites as visible light photocatalysts for selective organic transformations.

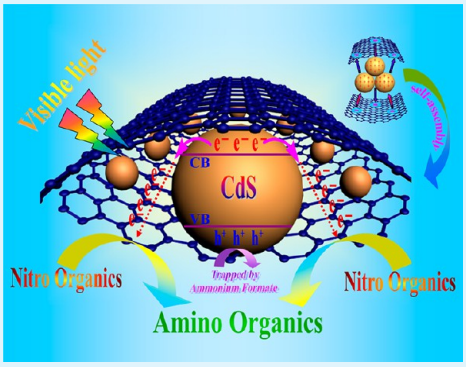

KEYWORDS: *CdS nanospheres (CdS NSPs), graphene (GR), electrostatic self-assembly, photocatalytic reduction, aromatic nitro organics*

INTRODUCTION

Graphene, which consists of a one-atom-thick planar sheet comprising an sp^2-bonded carbon structure with exceptionally high crystal and electronic quality, is a novel material that has emerged as a rapidly rising star in the field of material science.[1−4] Ever since its discovery in 2004,[5] graphene has been making a profound impact in many areas of science and technology due to its remarkable physicochemical properties. Especially, graphene possesses a high thermal conductivity (5000 W m^{-1} K^{-1}), offers an excellent mobility of charge carriers at room temperature (200 000 cm^2 V^{-1} s^{-1}), exhibits an extremely high theoretical specific surface area (2600 m^2 g^{-1}), and can be produced on a large scale at low cost.[2,6−9] Currently, it has been regarded as an important building block for synthesizing various functional composite materials. Notably, graphene (GR)-based semiconductor photocatalysts have attracted extensive attention because of their promising potential for conversion of solar to chemical energy.[9−16] So far, GR-based semiconductor nanocomposite photocatalysts are mainly focused on "nonselective" degradation of pollutants (dyes and volatile organic pollutant), photocatalytic destruction of bacteria and minuscule animals and water splitting to hydrogen.[9−14,17−34] In contrast, research work on utilizing GR-based semiconductor nanocomposites for photocatalytic "selective" redox reaction is relatively limited. Recently, our group has reported that GR-CdS, GR-TiO_2, and GR-ZnS photocatalysts can be used as a visible light photocatalyst for aerobic selective oxidation of alcohols to aldehydes and oxidation of alkenes to epoxides.[15,35−37] On the other hand, GR-based semiconductor nanocomposites have been demonstrated to exhibit much higher photocatalytic activity than bare semiconductors for selective photoreduction of CO_2 to CH_4 under both UV light and visible light irradiation.[38,39] These pioneering research works have strongly demonstrated that

Received: February 6, 2013
Accepted: April 18, 2013
Published: April 18, 2013

GR-based semiconductor nanocomposites hold great growth promise for heterogeneous photocatalytic selective redox transformations under ambient conditions. In addition, compared with selective oxidation reactions, photocatalytic selective reduction reactions are less frequently investigated over GR-based semiconductor composites. Therefore, it is of high interest to explore photocatalytic selective reduction driven by GR-based semiconductor composites.

It has been generally recognized that the fate and transfer of photogenerated electrons from semiconductor under light irradiation play an important role in the efficiency in triggering photocatalytic selective reduction reaction.[40−42] On account of superior electron conductivity and mobility of GR, the introduction of GR into the matrix of pure semiconductor via an appropriate manner should in principle boost the transfer and prolong the lifetime of the electrons photoexcited from semiconductor, which thus is able to drive selective reduction process more efficiently. Therefore, it could be reasonably expected that GR-based semiconductor nanocomposites have a great, promising potential for photocatalytic selective reduction reaction. However, research works available in the literature regarding photocatalytic reduction are mainly focused on the gas phase photoreduction of CO_2 for improved solar fuel production.[38,39] In contrast, it is still not available for the utilization of GR-based semiconductor composites photocatalysts for liquid phase selective reduction of nitro organics to amino organics in water, which is one of the significant synthetic reactions in organic chemistry.

Among the abundant GR-based semiconductor composites, CdS/GR hybrid composites have widely received attention and been successfully synthesized for the study of optical, electronic properties or application in photoelectrochemical cells, photocatalytic hydrogen evolution, and selective oxidation of alcohols.[22,30,35,43−52] Nevertheless, few research works report the utilization of CdS/GR composites for photocatalytic selective reduction of aromatic nitro organics, an important organic transformation. Furthermore, it should be noted that most of the CdS/GR composites are mainly prepared via in situ growth strategy, which can avoid the agglomeration of the CdS nanoparticles on the two-dimensional (2D) GR sheets and increase the interfacial contact between CdS and GR. On the other hand, increasing interest has also been devoted to fabricating GR-based nanocomposite photocatalysts by developing new synthetic strategies, among which the electrostatic self-assembly strategy has specific advantages on controlling the morphology of the semiconductor in a uniform manner, while this approach can also meet the needs for a good interfacial contact between semiconductor and the GR sheets.[53,54] Importantly, this strategy skillfully utilizes the negatively charged surface of GO colloids, which can be ascribed to the deprotonation of the carboxyl groups (—COOH) during the dialysis process in the synthesis of GO.[55,56] As a matter of fact, until now, the report on synthesis of uniform CdS nanospheres/graphene (CdS NSPs/GR) by such a simple self-assembly strategy, in terms of the electrostatic interaction of negatively charged GO and positively charged semiconductor, has been lacking.

In this paper, we have newly fabricated CdS nanospheres/graphene (CdS NSPs/GR) hybrid nanocomposites via a facile two-step wet chemistry process, i.e., electrostatic assembly of positively charged CdS nanospheres (CdS NSPs) with negatively charged graphene oxide (GO) followed by GO reduction to GR via a hydrothermal treatment. The as-obtained CdS NSPs/GR nanocomposites are able to exhibit a very stable, much higher photocatalytic performance than bare CdS NSPs toward selective reduction of nitro organics to amino organics in water under visible light irradiation. The significant photoactivity enhancement of CdS NSPs after coupling with GR is mainly attributed to the excellent electron conductivity of GR which acts as a two-dimensional (2D) network of an electron reservoir to accept and shuttle electrons photogenerated from the semiconductor CdS NSPs. As a result, the separation and lifetime of electron−hole pairs are improved, which thus contributes to the enhanced photoactivity. In addition, no apparent photodegradation of GR is observed in the current reaction system. This work provides a first example to use uniform CdS NSPs/GR nanocomposites as visible light photocatalyst for selective reduction of nitro organics to corresponding amino organics in water. It is anticipated that our current work could promote us to efficiently harness such a simple and efficient electrostatic self-assembly strategy to synthesize GR-based semiconductor composites with controlled morphology and, significantly, widen the application of CdS/GR and other GR-based semiconductor nanocomposites photocatalysts for selective organic reduction transformations.

EXPERIMENTAL SECTION

Materials. All reagents were analytical grade and used without further purification. Cadmium acetate dihydrate ($Cd(CH_3COO)_2{\cdot}2H_2O$), thiourea ($NH_2CSNH_2$), (3-aminopropyl)-triethoxysilane ($C_9H_{23}NO_3Si$, APTES), graphite powder, sulfuric acid (H_2SO_4), nitric acid (HNO_3), hydrochloric acid (HCl), potassium persulfate ($K_2S_2O_8$), phosphorus pentoxide (P_2O_5), hydrogen peroxide, 30% (H_2O_2), potassium permanganate ($KMnO_4$), and ethanol (C_2H_6O) were obtained from Sinopharm Chemical Reagent Co., Ltd. (Shanghai, China). Deionized water used in the synthesis was from local sources.

Preparation. The uniform CdS NSPs/GR nanocomposites have been fabricated by a facile and efficient electrostatic self-assembly method, followed by hydrothermal reduction of GO with deionized water solvent, as illustrated in Scheme 1. *(I) Fabrication of uniform CdS nanospheres (CdS NSPs).* Uniform CdS NSPs were obtained through a facile hydrothermal method.[57] The detail of the typical process is presented in the Supporting Information. *(II) Synthesis of graphene oxide (GO).* GO was synthesized from natural graphite powder by a modified Hummers method, which was also used in our previous

Scheme 1. Schematic Flowchart for Electrostatic Self-Assembly of Uniform CdS NSPs/GR Nanocomposites, Followed by GO Reduction via a Hydrothermal Treatment

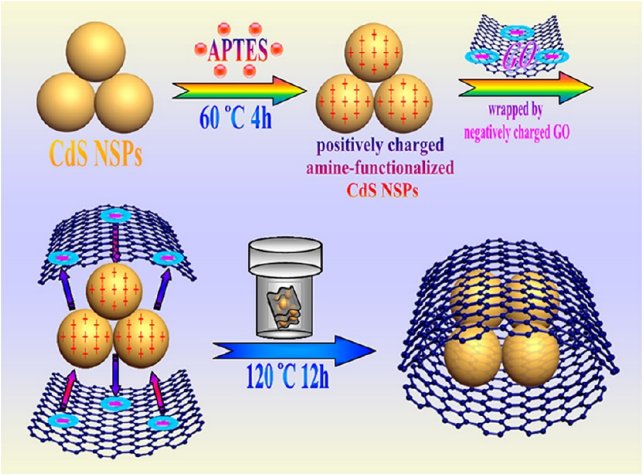

studies.[29,36] The detail of the typical process is presented in the Supporting Information. *(III) Synthesis of uniform CdS NSPs/GR nanocomposites by electrostatic self-assembly of CdS NSPs on the framework of GR.* 0.4 g CdS NSPs was first dispersed in 200 mL of ethanol by sonication for 30 min. Then, APTES (2 mL) was added, heated, and refluxed for 4 h. For reference, the structural formula of APTES has been displayed in the Supporting Information. APTES-treated CdS NSPs were sufficiently rinsed with ethanol to wash away any remaining APTES moiety. A negatively charged GO suspension (0.2 mg/mL) was added into a positively charged amine-functionalized CdS NSPs dispersion at the weight ratio of GO to CdS NSPs at 0.02:1, 0.05:1, and 0.1:1 under vigorous stirring at pH = 6. After mixing for 30 min, the mixture was centrifuged and washed with deionized water. For the reduction of GO to GR, a hydrothermal process was used as follows.[15] CdS NSPs/GO (0.2 g) nanocomposites with different weight addition ratios of GR were dispersed in deionized water (80 mL) and then autoclaved in a Teflon-lined stainless steel vessel at 120 °C for 12 h, which allows sufficient reduction of GO to GR. Next, the products were cooled to room temperature and recovered by filtration, washed by water, and fully dried at 333 K in an oven to obtain the final CdS NSPs/GR nanocomposites with different weight addition ratios of GR, namely, 2, 5, and 10% CdS NSPs/GR nanocomposites.

Characterization. Zeta potentials (ξ) measurements of the samples were determined by dynamic light scattering analysis (Zeta sizer 3000HSA) at room temperature of 25 °C. In brief, 25 mg of the sample was diluted to 50 mL of deionized water to obtain a concentration of ca. 500 mg/L in an aqueous solution. The pH adjustment was achieved by diluted 0.1 M HCl or NaOH aqueous solution when the zeta potential of the sample was measured as a function of pH value. The crystal phase properties of the samples were analyzed with a Bruker D8 Advance X-ray diffractometer (XRD) using Ni-filtered Cu Kα radiation at 40 kV and 40 mA in the 2θ, ranging from 5° to 80° with a scan rate of 0.02° per second. Field-emission scanning electron microscopy (FESEM) was used to determine the morphology of the samples on a FEI Nova NANOSEM 230 spectrophotometer. Transmission electron microscopy (TEM) images were obtained using a JEOL model JEM 2010 EX instrument at an accelerating voltage of 200 kV. Tapping-mode atomic force microscopy (AFM) measurements have been performed on a Nanoscope IIIA system in our previous work.[15] The sample for AFM imaging is prepared by depositing suspensions of graphene oxide (GO) in ethanol on a freshly cleaved mica surface. X-ray photoelectron spectroscopy (XPS) measurements were carried out on a Thermo Scientific ESCA Lab250 spectrometer which consists of a monochromatic Al Kα as the X-ray source, a hemispherical analyzer and sample stage with multiaxial adjustability to obtain the surface composition of the sample. All of the binding energies were calibrated by the C 1s peak at 284.6 eV. The details of XPS fitting are as follows: choosing Smart subtraction for the peak background subtraction and Gaussian shape as the shape of the peaks used for the deconvolution. Raman spectroscopic measurements were performed on a Renishaw inVia Raman System 1000 with a 532 nm Nd:YAG excitation source at room temperature. The Fourier transformed infrared spectroscopy (FTIR) was performed on a Nicolet Nexus 670 FTIR spectrophotometer at a resolution of 4 cm^{-1}. The Brunauer–Emmett–Teller (BET) specific surface area (S_{BET}) of the samples was analyzed by nitrogen adsorption in a Micromeritics ASAP 2020 apparatus. The electrochemical analysis was carried out in a conventional three-electrode cell using a Pt plate and an Ag/AgCl electrode as the counter electrode and reference electrode, respectively. The electrolyte was 0.2 M Na_2SO_4 aqueous solution without additive (pH = 6.8). The working electrode was prepared on indium–tin oxide (ITO) glass which was cleaned by sonication in ethanol for 30 min and dried at 353 K. The boundary of ITO glass was protected using scotch tape. A 5 mg sample was dispersed in 0.5 mL of N,N-dimethylflormamide (DMF, supplied from Sinopharm Chemical Reagent Co., Ltd.) by sonication to get slurry. The slurry was spread onto the pretreated ITO glass. After air drying, the working electrode was further dried at 393 K for 2 h to improve adhesion. Then the scotch tape was unstuck, and the uncoated part of the electrode was isolated with epoxy resin. The exposed area of the working electrode was 0.25 cm^2. The photocurrent measurements were taken on a BAS Epsilon workstation without bias. The electrochemical impedance spectroscopy experiments were conducted on a Precision PARC workstation. The photoluminescence (PL) spectra for solid samples were investigated on an Edinburgh FL/FS900 spectrophotometer with an excitation wavelength of 468 nm.

Photocatalytic Activity. In a typical photocatalytic reaction, a 300 W Xe arc lamp (PLS-SXE 300, Beijing Perfect light Co., Ltd.) with a UV–CUT filter to cut off light of wavelength λ < 420 nm was used as the irradiation source. Fifteen mg of the samples was added into 30 mL of the aromatic nitro compounds solution (20 $mg{\cdot}L^{-1}$) in a quartz vial. Before visible light illumination, the above suspension was stirred in the dark for 1 h to ensure the establishment of adsorption–desorption equilibrium between the sample and reactant. During the process of the reaction, 3 mL of the sample solution was collected at a certain time interval and centrifuged to remove the catalyst completely at 12000 rmp. Afterward, the solution was analyzed on a Varian ultraviolet–visible light (UV–vis) spectrophotometer (Cary–50, Varian Co.). The whole experimental process was conducted under N_2 bubbling at the flow rate of 80 $mL{\cdot}min^{-1}$.

RESULTS AND DISCUSSION

Electrostatic self-assembly of uniform CdS NSPs/GR nanocomposites has been performed by partly wrapping uniform CdS NSPs with graphene oxide (GO), followed by GO reduction via a hydrothermal treatment, which is displayed in Figure 1(A) and Scheme 1. As shown in Figure 1(B) and (C),

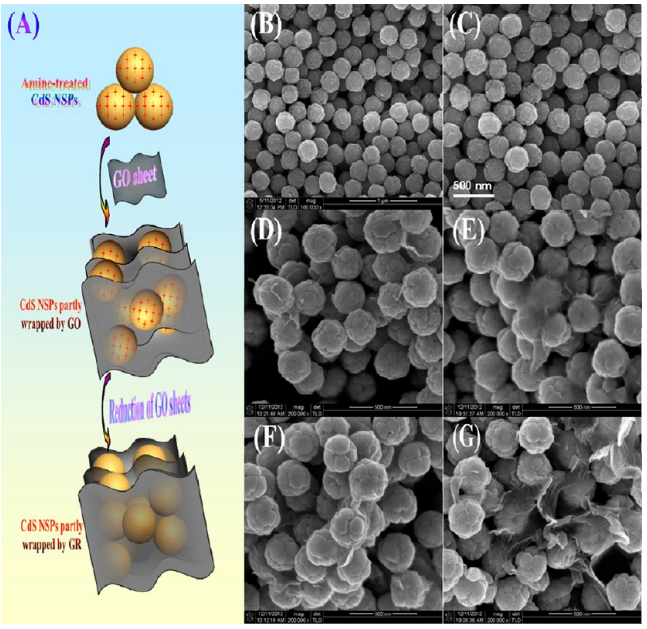

Figure 1. Schematic illustration of synthesis steps for GR-partly wrapped CdS NSPs and corresponding SEM images. (A) Synthesis steps of GR-partly wrapped CdS NSPs. (B) and (C) SEM images of bare CdS NPs prepared by hydrothermal method. (D) and (E) SEM images of GO-partly wrapped CdS NSPs. (F) and (G) SEM images of GR-partly wrapped CdS NSPs.

uniform CdS NSPs with an average diameter of 240 nm have been obtained through a hydrothermal process. With the modification by (3-aminopropyl)triethoxysilane (APTES), the surface of CdS NSPs has amine functional groups, by which the positively charged CdS NSPs are obtained. The zeta potential measurement of GO reveals a significant negatively charged surface along with excellent stabilization in the whole pH regime (1–10), as displayed in Figure S1 (Supporting

dx.doi.org/10.1021/am4010286 | ACS Appl. Mater. Interfaces 2013, 5, 4309–4319

Information). The stabilization of GO colloids in this pH range is due to electrostatic repulsions between charged GO. The negatively charged surface of GO colloids is due to the deprotonation of the carboxyl groups (—COOH) during the dialysis process in the synthesis of GO,[55,56] which establishes a solid and efficient basis for electrostatic attraction with the positively charged CdS NSPs.

The GO-partly wrapped uniform CdS NSPs can then be achieved by coassembly of positively charged CdS NSPs with negatively charged GO nanosheets (CdS NSPs/2% GO in Figure 1(D) and CdS NSPs/5% GO in Figure 1(E)) in an aqueous phase with the control of pH = 6. Followed by a hydrothermal process of reduction of GO to GR, the uniform CdS NSPs/GR nanocomposites (CdS NSPs/2% GR in Figure 1(F) and CdS NSPs/5% GR in Figure 1(G)) are obtained. The SEM characterization suggests a good interfacial contact formed between the uniform CdS NSPs and the GR sheets. Furthermore, the hydrothermal treatment process of GO reduction hardly affects the well-defined spherical morphology of uniform CdS NSPs, manifesting that such a simple, electrostatic self-assembly strategy has the dual advantages on maintaining the original uniform morphology of semiconductor CdS NSPs and, simultaneously, achieving the good interfacial contact.

It can be inferred from the SEM results that close interfacial contact between CdS NSPs and GR is achieved, which can be further evidenced by transmission electron microscopy (TEM) analysis. For CdS NSPs/5% GR nanocomposite shown in Figure 2, GR sheets-wrapped CdS NSPs like core@shell

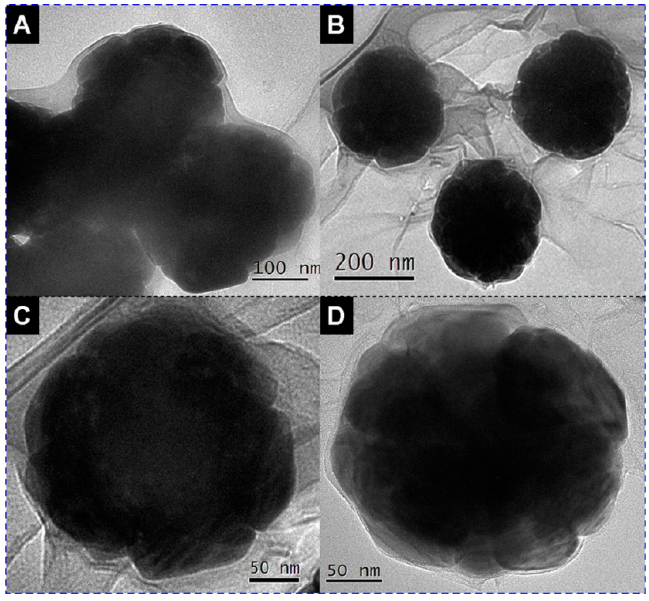

Figure 2. TEM images of CdS NSPs/5% GR nanocomposite.

structure are constructed, manifesting that the intimate interfacial contact between CdS NSPs and GR sheets is achieved via such a simple, electrostatic self-assembly strategy, which is in agreement with the SEM results. The joint SEM and TEM characterization faithfully verifies such a sufficient interfacial contact formed between the CdS NSPs and the GR sheets. Since the transfer process of charge carriers in GR-semiconductor nanocomposites is intimately related with the interfacial interaction between GR and the semiconductor,[15,36−39,58−68] it could be expected that such an intimate interfacial contact for the CdS NSPs/5% GR nanocomposite should favor the photogenerated charge carrier transfer process across the interface between CdS NSPs and GR upon visible light irradiation. In addition, it is established that such a GR-wrapped bacteria structure with a close interfacial contact between GR and bacteria is also beneficial for the inactivation of bacteria.[32]

The XRD patterns of GO, GR, and the CdS NSPs/GR nanocomposites are shown in Figure 3. It can be seen that GO

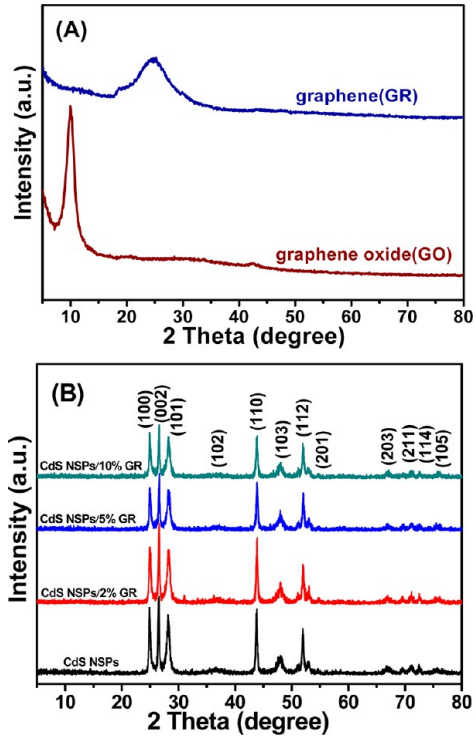

Figure 3. XRD patterns of the samples of GR and GO (A) and the samples of blank CdS NSPs and CdS NSPs/GR nanocomposites with different weight addition ratios of GR (B).

shows a sharp diffraction peak at 2θ value of ca. 10.1°. For the GR obtained from the hydrothermal reduction, the diffraction peak at ca. 10.1° disappears and a very broad diffraction peak at 2θ of ca. 25.0° appears, which means that GO sheets have been effectively exfoliated from the raw graphite, and, after hydrothermal reduction, almost all GO sheets have been transformed to GR with a random packing and significantly less functionalities.[26,29] For the CdS NSPs/GR nanocomposites with different weight addition ratios of GR, they show similar XRD patterns to blank CdS NSPs. The peaks located at ca. 24.8, 26.5, 28.2, 36.6, 43.7, 47.9, 50.9, 51.8, 52.8, 66.8, 69.2, 70.9, 72.3, and 75.4° are distinctly indexed to the (100), (002), (101), (102), (110), (103), (200), (112), (201), (203), (210), (211), (114), and (105) crystal planes of greenokite structure CdS (JCPDS No. 41-1049) with a hexagonal phase, respectively. Notably, no diffraction peaks for GR can be observed in the nanocomposites of CdS NSPs/GR, which might be due to the low amount and relatively low diffraction intensity of GR in the nanocomposites of CdS NSPs/GR.[15] On the other hand, the main characteristic peak of GR at ca. 25.0° may also be overlapped with the (100) peak of hexagonal CdS.

The efficient reduction of GO to GR after the hydrothermal treatment can also be evidenced by the contrast comparison of

the C 1s X-ray photoelectron spectra (XPS) of GO and CdS NSPs/GR (here, taking CdS NSPs/5% GR as an example), which is displayed in Figure 4. For the bare GO, the C 1s XPS

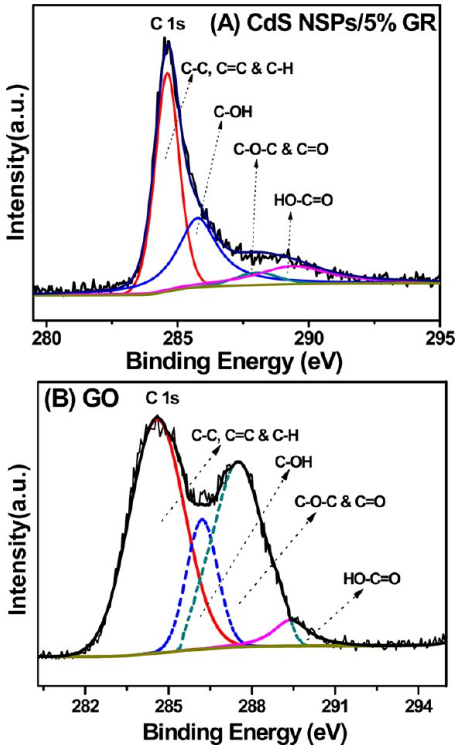

Figure 4. C 1s X-ray photoelectron spectra (XPS) of CdS NSPs/5% GR nanocomposite (A) and the original GO (B).

spectra suggest the abundance of various oxygen-containing functional groups on the GO surface. For the CdS NSPs/5% GR nanocomposite, the significant loss of oxygen-containing functional groups is observed based on the C 1s XPS spectra in Figure 4(A), which indicates the sufficient reduction of GO to GR after coupling CdS NSPs with GO via a hydrothermal reduction treatment.[15,36] The XPS result is in good agreement with the Fourier transformed infrared spectroscopy (FTIR), as shown in Figure S2 (Supporting Information), which also indicates the hydrothermal treatment is able to efficiently reduce GO to GR. Figure 5(A) shows the Raman spectra of GO, graphite (GP) and CdS NSPs/5% GR nanocomposite. Of particular note is the intensity ratio of the D band (~1350 cm^{-1}) and G band (~1590 cm^{-1}), I_D/I_G, which is a measure of the relative concentration of local defects or disorders (particularly the sp^3-hybridized defects) compared to the sp^2-hybridized GR domains.[15,36,38] It can be seen that the I_D/I_G ratio is 1.03 for GO. After the hydrothermal reaction, the I_D/I_G ratio is decreased to 0.96, thus indicating more graphitization of the CdS NSPs/5% GR nanocomposite resulting from the hydrothermal reduction process. In addition, as compared to Raman spectra of GP, we can draw the conclusion that it is graphene rather than graphite in the hybrid nanocomposites. To verify the number of graphene layers in the produced nanocomposites, we have analyzed the variation of the 2D band at ~2700 cm^{-1},[38,69−72] as displayed in Figure 5(B). The observed spectrum variation is in agreement the previously reported data.[69,70] The 2D peaks of the CdS NSPs/5% GR nanocomposite powders and GR powders are found with lower intensity than graphite powders, manifesting the restack and

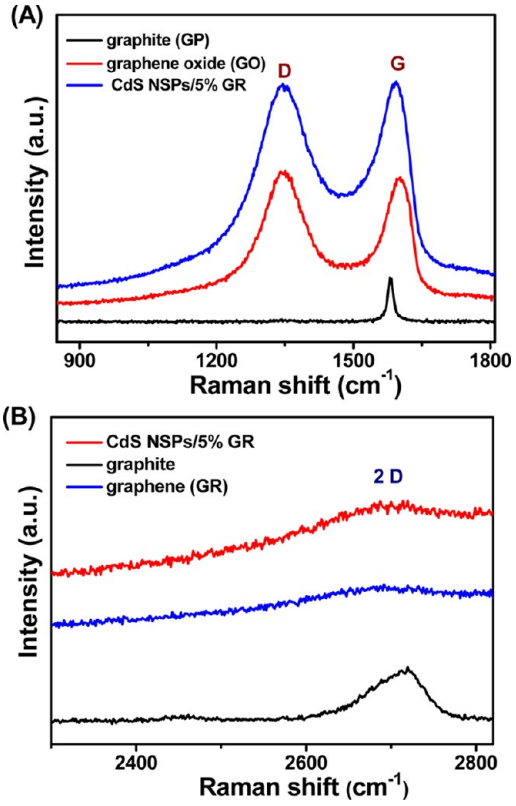

Figure 5. Raman spectra of GO, graphite (GP), and CdS NSPs/5% GR nanocomposite (A) and GR, GP, and CdS NSPs/5% GR nanocomposite (B) at room temperature.

agglomeration of GR sheets occur in the reduction of GO to GR. Compared with previous works,[69−72] it can be referred from the intensity and location of 2D peak for CdS NSPs/5% GR that the number of GR layers in the nanocomposite is not single or bistratal but multilayer. In addition, atomic force microscopy (AFM) images and height profiles of GO are provided in Figure S3 (Supporting Information). The results demonstrate that GO used in our experiment are almost single-layer, which can be widely used in fabricating GR-based semiconductor photocatalysts to increase the interfacial contact and synergistic interaction between GR and semiconductor. Nevertheless, in the synthesis of GR-based semiconductor nanocomposites, the GR prepared from reduction of GO, which was prepared by removing the hydrophilic oxygen functional groups from carbon planar of GO sheets, would easily stack and agglomerate. Thus, it is understandable that graphene in the GR-based nanocomposites is hardly single-layer, thus leading to the low intensity of a 2D peak in the Raman spectra.

The photocatalytic activities of uniform CdS NSPs/GR nanocomposites have been evaluated by selective reduction of aromatic nitro organics to corresponding amino organics in the aqueous phase with the addition of ammonium formate as quencher for photogenerated holes and N_2 purge under visible light irradiation. Figure 6(A) shows the photocatalytic activity of blank CdS NSPs and uniform CdS NSPs/GR nanocomposites with different weight addition ratios of GR toward photocatalytic selective reduction of 4-nitroaniline (4-NA). The CdS NSPs/GR nanocomposites exhibit much higher photocatalytic activity than bare CdS NSPs and the photocatalytic reduction efficiency of 4-NA follows the order: CdS NSPs/5%

dx.doi.org/10.1021/am4010286 | ACS Appl. Mater. Interfaces 2013, 5, 4309−4319

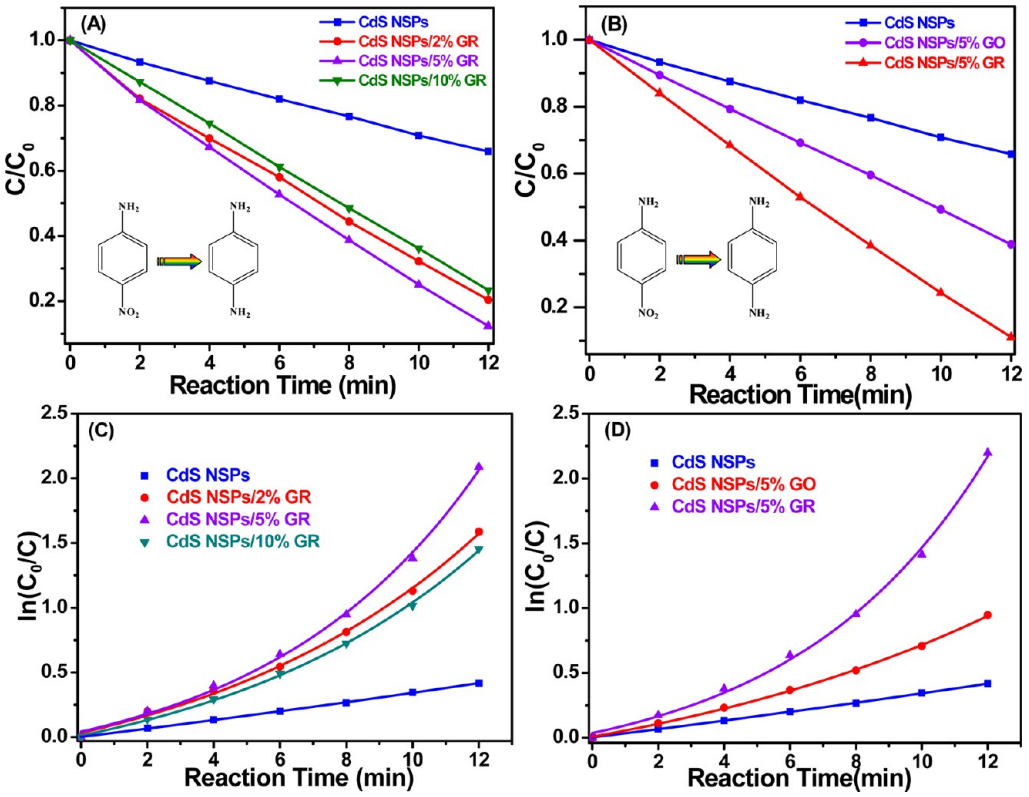

Figure 6. Photocatalytic selective reduction of 4-NA to PPD over bare CdS NSPs and the CdS NSPs/GR nanocomposites with different weight additions of GR (A) and (C) and photocatalytic selective reduction of 4-NA to PPD over CdS NSPs, CdS NSPs/5% GO, and CdS NSPs/5% GR (B) and (D), under visible light irradiation.

GR > CdS NSPs/2% GR > CdS NSPs/10% GR > bare CdS NSPs. As displayed in Figure S4 (Supporting Information), the absorption at 380 nm decreases, and absorption at 240 and 300 nm increases concomitantly, which can be ascribed to the reduction of 4-NA and the formation of p-phenylenediamine (PPD).[73] This is further corroborated by the high performance liquid chromatograph (HPLC) spectra, as shown in Figure S5. To study the influence of efficient reduction of GO to GR on the photocatalytic activity, the photocatalytic performance of CdS NSPs/5% GO has been performed for reduction of 4-NA to PPD, which is depicted in Figure 6(B). As expected, CdS NSPs/5% GR exhibits higher photoactivity than CdS NSPs/5% GO, which suggests that efficient reduction of GO to GR plays a positive role in improving the photocatalytic activity for reduction of 4-NA. In addition, the kinetics of the reduction of 4-NA to PPD based on the above data has been investigated. Different from the degradation of dyes in previous studies,[74] the reduction kinetics of nitro organics can be fitted by the ExpAssoc model from nonlinear curve fit based on the experimental data. As displayed in Figure 6(C) and (D), it is clear that the CdS NSPs/5% GR nanocomposite exhibits the best photocatalytic reduction efficiency among all the samples, which is in accordance with the photocatalytic activities in Figure 6(A) and (B). Importantly, these reach a consensus that the induction of an appropriate amount of GR into the matrix of CdS NSPs can result in obvious enhancement of photocatalytic performance for selective reduction of 4-NA.

To ensure if such an enhancement of photocatalytic activity toward reduction of nitro organics is general, we have further investigated the photocatalytic performance of bare CdS NSPs and CdS NSPs/5% GR toward selective reduction of other aromatic nitro compounds with various substituent groups, including 4-nitrophenol, 2-nitrophenol, 2-nitroaniline, 1-chloro-4-nitrobenzene, 4-nitroanisole, and 1-bromo-4-nitrobenzene. As can be clearly reflected by the data in Figure 7A–F, such a similar significantly enhanced activity trend has been observed, similar to that for selective reduction of 4-NA to PPD. Since the photocatalytic reduction efficiency is intimately related with the fate and transfer of photogenerated electrons, the highly enhanced photocatalytic performance, as observed for photoreduction of aromatic nitro organics, could be attributed to the fact that the addition of GR into the matrix of CdS NSPs would remarkably improve the fate and transfer of photogenerated electron–hole pairs from CdS NSPs. In addition, it should be noted that, in our reaction system, the photogenerated positive holes are quenched by the addition of ammonium formate, thus offering an adequate opportunity of spatial contact between photogenerated electrons and reactants (aromatic nitro organics). Besides, the presence of GR could also increase the concentration of the reactants accumulating over the surface of photocatalysts. These integrative factors can result in the increased photocatalytic activity of CdS NSPs/5% GR as compared to bare CdS NSPs. The above inferences have been sufficiently evidenced by the following characterization of photocatalysts CdS NSPs/5% GR and bare CdS NSPs, which include photoelectrochemical analysis, photoluminescence (PL) spectra, and surface area measurement.

Table S1 shows the Brunauer–Emmett–Teller (BET) surface area and pore volume of the samples bare CdS NSPs and CdS NSPs/5% GR. It is seen that the introduction of GR gives rise to a larger surface area and total pore volume than those of bare CdS NSPs. The increased surface area and pore

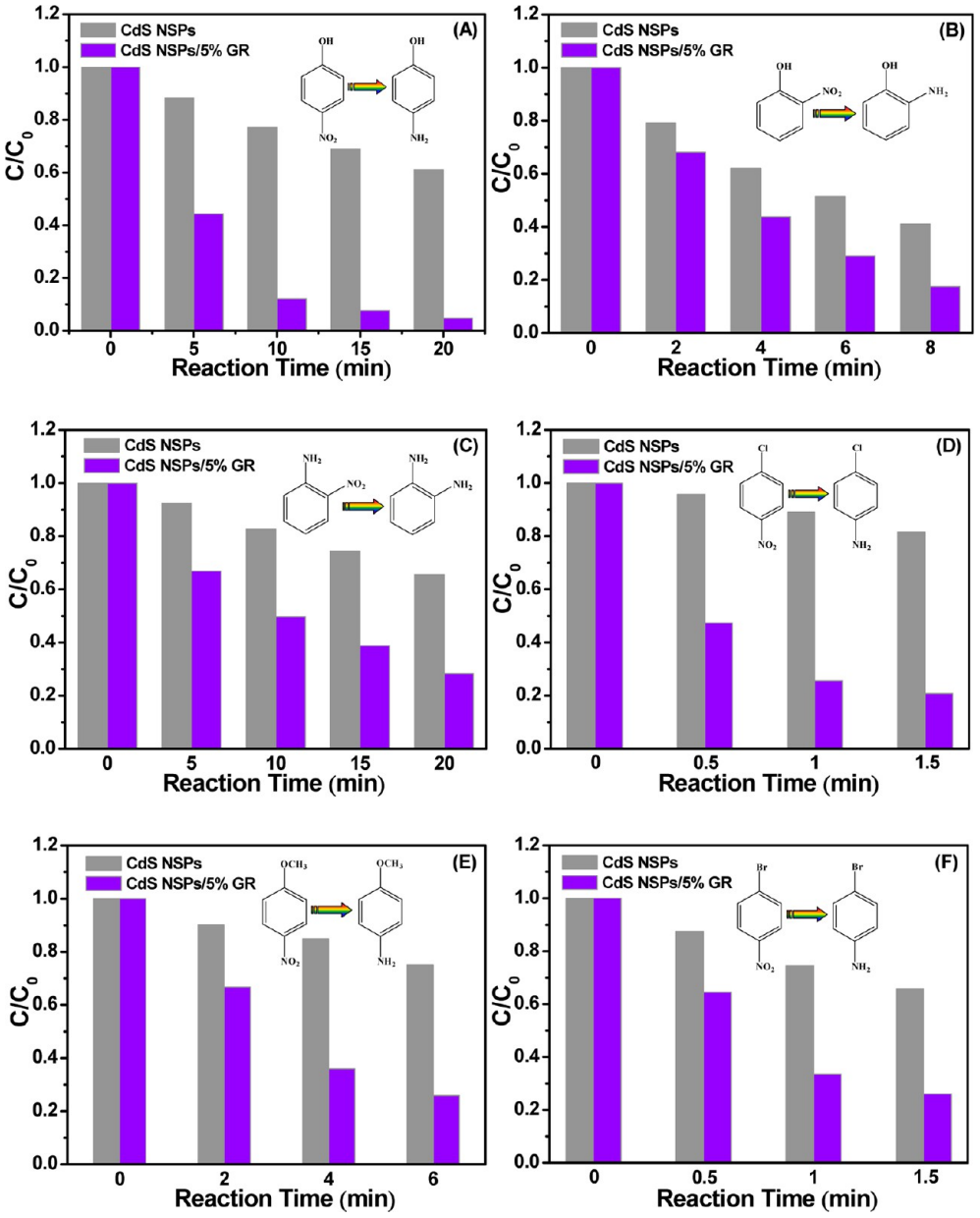

Figure 7. Photocatalytic performance of CdS NSPs, CdS NSPs/5% GO nanocomposite for photocatalytic reduction of other aromatic nitro compounds under ambient conditions: (A) 4-nitrophenol; (B) 2-nitrophenol; (C) 2-nitroaniline; (D) 1-chloro-4-nitrobenzene; (E) 4-nitroanisole; (F) 1-bromo-4-nitrobenzene.

volume lead to the difference in the adsorptivity of samples toward aromatic nitro organics, which is faithfully verified by the results of adsorption experiments in the dark for 4-NA. As displayed in Figure S6 (Supporting Information), it can be seen that the introduction of GR can increase the adsorptivity of the samples for reactants, which is beneficial for the undergoing of the targeted reactions.[26,29,35,36] In addition, the adsorptivity enhancement could also result from the $\pi-\pi$ conjugation between aromatic nitro organics and aromatic regions of graphene. Such an increased adsorptivity of CdS NSPs/5% GR nanocomposite is beneficial for reduction of aromatic nitro organics on the surface of photocatalyst under visible light irradiation.

Figure 8 shows the photocurrent of CdS NSPs/5% GR and bare CdS NSPs electrodes under visible light irradiation. It is clear to see that, due to the introduction of GR, the transient photocurrent response of CdS NSPs/5% GR is remarkably higher than bare CdS NSPs, suggesting the significantly enhanced life span over CdS NSPs/5% GR under visible light irradiation. This is also supported by the results of photoluminescence (PL) spectra, which is a well-known technique to study the fate of electron−hole pairs photogenerated from semiconductor.[15,35,37] It can be seen from Figure S7 (Supporting Information) that the PL intensity of CdS NSPs/5% GR is much weaker than CdS NSPs, indicating that the recombination of photogenerated electron−hole pairs is efficiently hampered after the integration of CdS NSPs with GR. To further determine the advantage of CdS NSPs/5% GR over CdS NSPs in improving the charge carriers transfer, electrochemical impedance spectra (EIS) Nyquist plot, a very useful tool to characterize the charge-carrier migration, has also been performed. It can be observed from Figure 9 that the CdS

dx.doi.org/10.1021/am4010286 | ACS Appl. Mater. Interfaces 2013, 5, 4309−4319

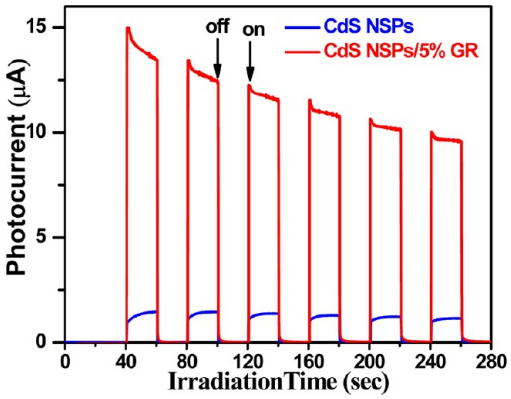

Figure 8. Transient photocurrent response of blank CdS NSPs and CdS NSPs/5% GR nanocomposite in 0.2 M Na_2SO_4 aqueous solution (pH = 6.8) without bias versus Ag/AgCl electrode.

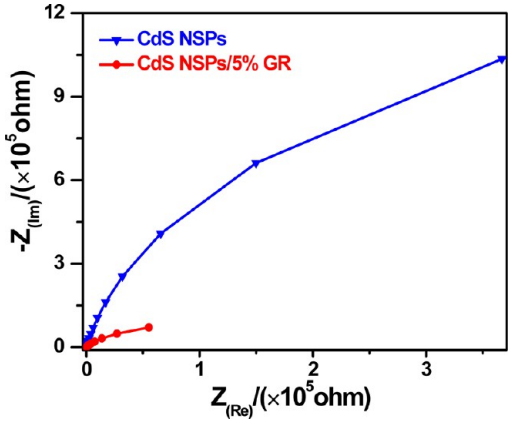

Figure 9. Nyquist impedance plots of blank CdS NSPs and CdS NSPs/5% GR nanocomposite under visible light irradiation in 0.2 M Na_2SO_4 aqueous solution (pH = 6.8).

NSPs/5% GR nanocomposite exhibits depressed semicircles at high frequencies compared with pure CdS NSPs, which manifests a decrease in the solid state interface layer resistance and the charge transfer resistance across the solid−liquid junction on the surface by forming nanocomposites of CdS NSPs with graphene.[75] Namely, the more efficient transfer of charge carriers is obtained over CdS NSPs/5% GR than CdS NSPs. On the other hand, it should be noted that, in our reaction system, the photogenerated positive holes are scavenged by the quenching agent of ammonium formate. Thus, the significantly improved lifetime and transfer of photogenerated electrons for CdS NSPs/5% GR can effectively lead to the enhanced photoactivity toward the sequential reduction of aromatic nitro organics to the target product amino organics.

Based on the above results, the introduction of GR into the matrix of CdS NSPs in CdS NSPs/5% GR nanocomposite is able to significantly improve the lifetime and transfer of photogenerated charge carriers and, thus, increase the contact efficiency of photogenerated electrons with reactants. In addition, the introduction of GR also improves the adsorptivity of CdS NSPs/5% GR toward reactants. These two integrative factors result in the significant enhancement of photocatalytic activity of CdS NSPs/5% GR toward reduction of aromatic nitro organics in water under visible light irradiation.

Compared with the photocatalytic activity, the stability of a photocatalyst is also of much importance for its application. In other words, attention should also be paid to prohibiting photocatalyst deactivation for a sustainable reuse.[76−83] Therefore, photocatalytic test on the reusability of the CdS NSPs/5% GR nanocomposite is necessary. It has been established that CdS generally suffers from photocorrosion due to the oxidation of CdS by its own photogenerated holes, especially in aqueous solution.[84,85] Zhu et al.[77,83] and Dai et al.[76] have reported effective photocorrosion inhibition of ZnO via hybridization with carbon materials (e.g., C_{60}, graphite-like carbon and carbon nanotube). Ma and co-workers[78] have synthesized CdS nanoparticles dotted on the surface of multiwalled carbon nanotubes, which could hamper the photocorrosion of CdS. Thus, the intimate interfacial contact between CdS NSPs and GR sheets could also inhibit the photocorrosion of CdS NSPs. In addition, photogenerated holes are quenched by the addition of ammonium formate, which also prevents the photocorrosion of CdS NSPs during the photocatalytic reaction. This inference is verified by no significant loss of photoactivity during five successive recycling tests for reduction of 4-NA over CdS NSPs/5% GR under visible light irradiation, as displayed in Figure 10.

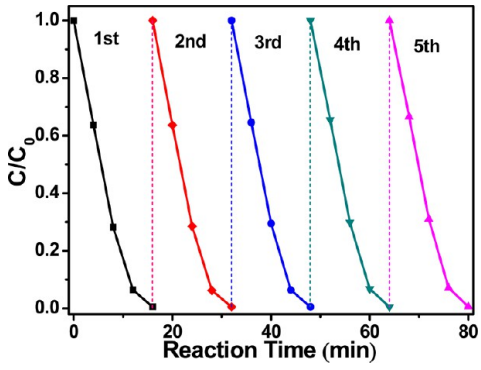

Figure 10. Recycling photocatalytic reduction of 4-NA over CdS NSPs/5% GR nanocomposite under visible light irradiation (λ > 420 nm) with the addition of ammonium formate as quencher for photogenerated holes and N_2 purge at room temperature in the aqueous phase.

The other issue that should be mentioned is concerning the possible degradation of GR during the photocatalytic reaction.[17,86] It has been shown that carbon bonds of graphene can be cut by oxidation.[87] Moreover, it has been reported that the local degradation of GR sheets results from active •OH radicals effectively produced by the photogenerated holes accumulated in the tip of the excited ZnO nanorods.[17] Therefore, the existence of the photogenerated holes may give rise to the photodegradation of GR. Nevertheless, in our reaction system, the addition of ammonium formate as quencher for photogenerated holes in photocatalytic selective reduction of nitro organics effectively inhibits the photodegradation of graphene in aqueous solution. Thus, the synergetic effect of the addition of GR and ammonium formate as quencher for photogenerated holes makes CdS NSPs/5% GR nanocomposite be a reusable and efficient catalyst for photocatalytic reduction of aromatic nitro compounds in water.

To ensure the decisive role of photogenerated electrons during reduction of aromatic nitro organics, we have performed the controlled experiments, using $AgNO_3$ as scavenger for

photogenerated electrons, for reduction of 4-NA over bare CdS NSPs and CdS NSPs/5% GR under visible light irradiation. The results are displayed in Figure 11. It is clear to see that no

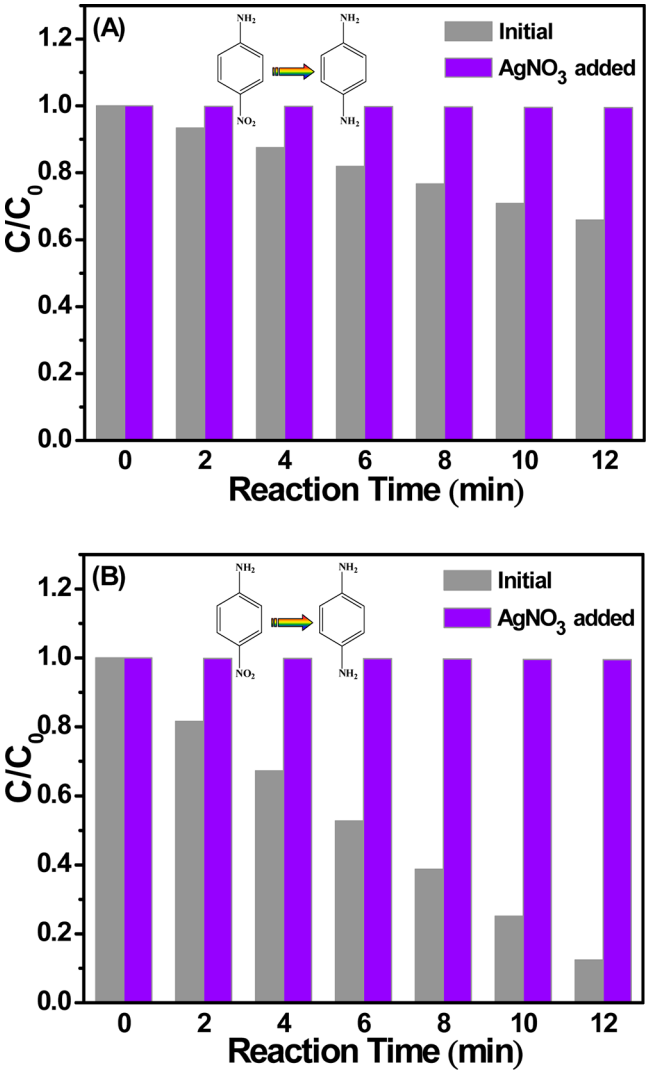

Figure 11. Controlled experiments for 4-NA reduction over CdS NSPs (A) and CdS NSPs/5% GR (B) using $AgNO_3$ as scavenger for photogenerated electrons under visible light irradiation (λ > 420 nm) with the addition of ammonium formate as quencher for photogenerated holes and N_2 purge at room temperature in the aqueous phase.

conversion of 4-NA is observed over both CdS NSPs/5% GR and bare CdS NSPs, which clearly indicates that the reduction reactions of aromatic nitro organics are driven by the photogenerated electrons under visible light irradiation. This is reasonable because the overall photoreduction of aromatic nitro organics to corresponding amino organics can be expressed by the following formula (taking photoreduction of 4-NA to PPD as an example).[41,73,88]

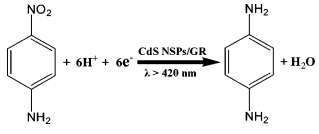

On the basis of the above results, a tentative reaction mechanism for photocatalytic selective reduction of aromatic nitro organics to corresponding amino organics over CdS NSPs/GR nanocomposites can be proposed as the following, which is schematically displayed in Figure 12. Under the

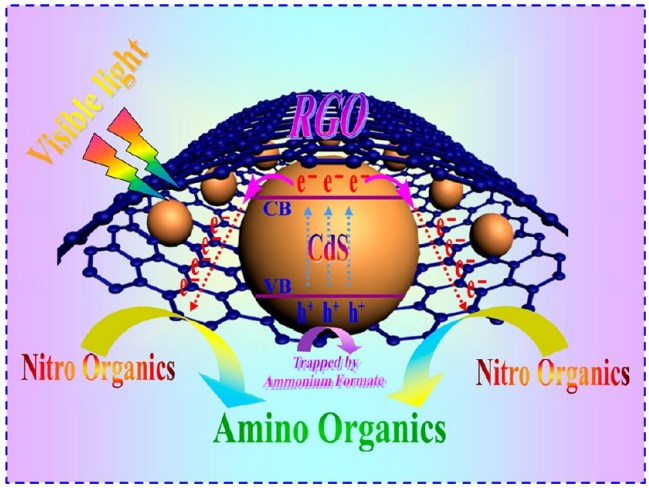

Figure 12. Schematic diagram illustrating the photocatalytic reduction process of aromatic nitro organics to corresponding amino organics over the CdS NSPs/GR nanocomposite under visible light irradiation (λ > 420 nm) with the addition of ammonium formate as quencher for photogenerated holes and N_2 purge at room temperature.

illumination of visible light, CdS NSPs in the CdS NSPs/GR photocatalyst is photoexcited to generate electron−hole pairs. Due to the introduction of GR, the work function of which is less negative than the conduction band of CdS (−0.08 V for GR vs NHE),[35,89,90] the photogenerated electrons can transfer from CdS to the GR sheets, thus prolonging the lifetime of the charge carriers. Simultaneously, the photogenerated holes are trapped by the quenching agent of ammonium formate. In addition, the N_2 purge provides an anaerobic atmosphere for the reaction. Thus, the aromatic nitro organics have no opportunity to undergo the oxidation reaction. Due to the presence of GR, the photogenerated electrons from CdS NSPs can easily transfer to the GR framework, by which the lifetime and transfer of photogenerated electrons is significantly improved. Meanwhile, the presence of GR also increases the accumulating concentration of nitro organics over the surface of CdS NSPs/GR nanocomposites. As a result, the adsorbed aromatic nitro organics can be effectively reduced to amino organics by accepting photogenerated electrons from CdS NSPs/GR under visible light irradiation.

CONCLUSION

In summary, we have successfully fabricated uniform CdS NSPs/GR hybrid nanocomposites via an electrostatic self-assembly route combined a facile hydrothermal process, during which GR and the intimate interfacial contact between CdS NSPs and the GR sheets are achieved. The CdS NSPs/GR hybrid nanocomposites are demonstrated to exhibit high visible light photocatalytic performance and excellent reusability toward selective reduction of aromatic nitro organics to corresponding amino organics in water. The high photocatalytic activity of CdS NSPs/GR hybrid nanocomposites can be ascribed to the increased adsorptivity, the improved lifetime and transfer of charge carriers (particularly for photogenerated

electrons), and the addition of ammonium formate as quencher for photogenerated holes. The photocorrosion of CdS and the photodegradation of GR in aqueous solution are not observed in our photocatalytic reduction reaction system. Thus, the CdS NSPs/GR nanocomposite can be a good reusable visible light catalyst for photoreduction of aromatic nitro organics. It is hoped that our current work could promote further interest in utilizing such a simple, efficient self-assembly strategy to synthesize GR-based semiconductor hybrids with controlled uniform morphology and good interfacial contact and, more significantly, widen the application of CdS/GR nanocomposites as visible light photocatalysts for selective organic reduction transformations.

■ ASSOCIATED CONTENT

Ⓢ Supporting Information

Experimental details for synthesis of CdS nanospheres (CdS NSPs) and graphene oxide (GO), zeta potentials analysis, Fourier transformed infrared spectroscopy (FTIR) spectra, atomic force microscopy (AFM) images and height profiles of GO, UV−vis absorption spectra of photocatalytic reduction of 4-NA, UV−vis absorption spectra of 4-NA over CdS NSPs and CdS NSPs/5% GR nanocomposite under adsorption equilibrium and column plot showing the remaining 4-NA in solution after being kept in the dark for 1 h until adsorption equilibrium of the 4-NA solution, high performance liquid chromatograph (HPLC) data, PL spectra of bare CdS NSPs and CdS NSPs/5% GR nanocomposite with an excitation wavelength of 468 nm, SEM images of CdS NSPs with different sizes, photocatalytic selective reduction of 4-NA to PPD over CdS NSPs with different sizes and corresponding CdS NSPs/GR nanocomposites. This material is available free of charge via the Internet at http://pubs.acs.org.

■ AUTHOR INFORMATION

Corresponding Author

*Phone/Fax: +86 591 83779326. E-mail: yjxu@fzu.edu.cn.

Notes

The authors declare no competing financial interest.

■ ACKNOWLEDGMENTS

The support by the National Natural Science Foundation of China (NSFC) (21173045, 20903023), the Award Program for Minjiang Scholar Professorship, the Natural Science Foundation (NSF) of Fujian Province for Distinguished Young Investigator Grant (2012J06003), Program for Changjiang Scholars and Innovative Research Team in Universities (PCSIRT0818), Program for Returned High-Level Overseas Chinese Scholars of Fujian province, and the Project Sponsored by the Scientific Research Foundation for the Returned Overseas Chinese Scholars, State Education Ministry, is gratefully acknowledged.

■ REFERENCES

(1) Chen, D.; Feng, H.; Li, J. *Chem. Rev.* **2012**, *112*, 6027−6053.
(2) Geim, A. K.; Novoselov, K. S. *Nat. Mater.* **2007**, *6*, 183−191.
(3) Li, D.; Kaner, R. B. *Science* **2008**, *320*, 1170−1171.
(4) Sykes, E. C. H. *Nat. Chem.* **2009**, *1*, 175−176.
(5) Novoselov, K. S.; Geim, A. K.; Morozov, S. V.; Jiang, D.; Zhang, Y.; Dubonos, S. V.; Grigorieva, I. V.; Firsov, A. A. *Science* **2004**, *306*, 666−669.
(6) Allen, M. J.; Tung, V. C.; Kaner, R. B. *Chem. Rev.* **2009**, *110*, 132−145.
(7) Geim, A. K. *Science* **2009**, *324*, 1530−1534.
(8) Stankovich, S.; Dikin, D. A.; Dommett, G. H. B.; Kohlhaas, K. M.; Zimney, E. J.; Stach, E. A.; Piner, R. D.; Nguyen, S. T.; Ruoff, R. S. *Nature* **2006**, *442*, 282−286.
(9) Xiang, Q.; Yu, J.; Jaroniec, M. *Chem. Soc. Rev.* **2012**, *41*, 782−796.
(10) An, X.; Yu, J. C. *RSC Adv.* **2011**, *1*, 1426−1434.
(11) Huang, X.; Qi, X.; Boey, F.; Zhang, H. *Chem. Soc. Rev.* **2012**, *41*, 666−686.
(12) Kamat, P. V. *J. Phys. Chem. Lett.* **2011**, *2*, 242−251.
(13) Lightcap, I. V.; Kosel, T. H.; Kamat, P. V. *Nano Lett.* **2010**, *10*, 577−583.
(14) Zhang, N.; Zhang, Y.; Xu, Y.-J. *Nanoscale* **2012**, *4*, 5792−5813.
(15) Zhang, Y.; Zhang, N.; Tang, Z.-R.; Xu, Y.-J. *ACS Nano* **2012**, *6*, 9777−9789.
(16) Xiang, Q.; Yu, J. *J. Phys. Chem. Lett.* **2013**, *4*, 753−759.
(17) Akhavan, O. *ACS Nano* **2010**, *4*, 4174−4180.
(18) Akhavan, O.; Ghaderi, E. *J. Phys. Chem. C* **2009**, *113*, 20214−20220.
(19) Chen, C.; Cai, W.; Long, M.; Zhou, B.; Wu, Y.; Wu, D.; Feng, Y. *ACS Nano* **2010**, *4*, 6425−6432.
(20) Fan, W.; Lai, Q.; Zhang, Q.; Wang, Y. *J. Phys. Chem. C* **2011**, *115*, 10694−10701.
(21) Iwase, A.; Ng, Y. H.; Ishiguro, Y.; Kudo, A.; Amal, R. *J. Am. Chem. Soc.* **2011**, *133*, 11054−11057.
(22) Li, Q.; Guo, B.; Yu, J.; Ran, J.; Zhang, B.; Yan, H.; Gong, J. R. *J. Am. Chem. Soc.* **2011**, *133*, 10878−10884.
(23) Ng, Y. H.; Lightcap, I. V.; Goodwin, K.; Matsumura, M.; Kamat, P. V. *J. Phys. Chem. Lett.* **2010**, *1*, 2222−2227.
(24) Pan, X.; Zhao, Y.; Liu, S.; Korzeniewski, C. L.; Wang, S.; Fan, Z. *ACS Appl. Mater. Interfaces* **2012**, *4*, 3944−3950.
(25) Xu, T.; Zhang, L.; Cheng, H.; Zhu, Y. *Appl. Catal., B* **2011**, *101*, 382−387.
(26) Chen, Z.; Zhang, N.; Xu, Y.-J. *CrystEngComm* **2013**, *15*, 3022−3030.
(27) Zhang, J.; Xiong, Z.; Zhao, X. S. *J. Mater. Chem.* **2011**, *21*, 3634−3640.
(28) Zhang, X.-Y.; Li, H.-P.; Cui, X.-L.; Lin, Y. *J. Mater. Chem.* **2010**, *20*, 2801−2806.
(29) Zhang, Y.; Tang, Z.-R.; Fu, X.; Xu, Y.-J. *ACS Nano* **2010**, *4*, 7303−7314.
(30) Jia, L.; Wang, D.-H.; Huang, Y.-X.; Xu, A.-W.; Yu, H.-Q. *J. Phys. Chem. C* **2011**, *115*, 11466−11473.
(31) Zhang, J.; Yu, J.; Jaroniec, M.; Gong, J. R. *Nano Lett.* **2012**, *12*, 4584−4589.
(32) Akhavan, O.; Ghaderi, E.; Esfandiar, A. *J. Phys. Chem. B* **2011**, *115*, 6279−6288.
(33) Akhavan, O.; Ghaderi, E.; Rahimi, K. *J. Mater. Chem.* **2012**, *22*, 23260−23266.
(34) Xiang, Q.; Yu, J.; Jaroniec, M. *J. Am. Chem. Soc.* **2012**, *134*, 6575−6578.
(35) Zhang, N.; Zhang, Y.; Pan, X.; Fu, X.; Liu, S.; Xu, Y.-J. *J. Phys. Chem. C* **2011**, *115*, 23501−23511.
(36) Zhang, Y.; Tang, Z.-R.; Fu, X.; Xu, Y.-J. *ACS Nano* **2011**, *5*, 7426−7435.
(37) Zhang, Y.; Zhang, N.; Tang, Z.-R.; Xu, Y.-J. *Phys. Chem. Chem. Phys.* **2012**, *14*, 9167−9175.
(38) Liang, Y. T.; Vijayan, B. K.; Gray, K. A.; Hersam, M. C. *Nano Lett.* **2011**, *11*, 2865−2870.
(39) Liang, Y. T.; Vijayan, B. K.; Lyandres, O.; Gray, K. A.; Hersam, M. C. *J. Phys. Chem. Lett.* **2012**, *3*, 1760−1765.
(40) Maldotti, A.; Andreotti, L.; Molinari, A.; Tollari, S.; Penoni, A.; Cenini, S. *J. Photochem. Photobiol., A* **2000**, *133*, 129−133.
(41) Tada, H.; Ishida, T.; Takao, A.; Ito, S. *Langmuir* **2004**, *20*, 7898−7900.
(42) Zhang, F.; Jin, R.; Chen, J.; Shao, C.; Gao, W.; Li, L.; Guan, N. *J. Catal.* **2005**, *232*, 424−431.
(43) Zhang, N.; Zhang, Y.; Yang, M.-Q.; Tang, Z.-R.; Xu, Y.-J. *J. Catal.* **2013**, *299*, 210−221.

(44) Chang, H.; Lv, X.; Zhang, H.; Li, J. *Electrochem. Commun.* **2010**, *12*, 483−487.
(45) Dufaux, T.; Boettcher, J.; Burghard, M.; Kern, K. *Small* **2010**, *6*, 1868−1872.
(46) Zhang, N.; Yang, M.-Q.; Tang, Z.-R.; Xu, Y.-J. *J. Catal.* **2013**, *303*, 60−69.
(47) Feng, M.; Sun, R.; Zhan, H.; Chen, Y. *Nanotechnology* **2010**, *21*, 075601.
(48) Nethravathi, C.; Nisha, T.; Ravishankar, N.; Shivakumara, C.; Rajamathi, M. *Carbon* **2009**, *47*, 2054−2059.
(49) Pham, T. A.; Choi, B. C.; Jeong, Y. T. *Nanotechnology* **2010**, *21*, 465603.
(50) Wang, K.; Liu, Q.; Wu, X.-Y.; Guan, Q.-M.; Li, H.-N. *Talanta* **2010**, *82*, 372−376.
(51) Wang, P.; Jiang, T.; Zhu, C.; Zhai, Y.; Wang, D.; Dong, S. *Nano Res.* **2010**, *3*, 794−799.
(52) Wu, J.; Bai, S.; Shen, X.; Jiang, L. *Appl. Surf. Sci.* **2010**, *257*, 747−751.
(53) Chen, J. S.; Wang, Z.; Dong, X. C.; Chen, P.; Lou, X. W. *Nanoscale* **2011**, *3*, 2158−2161.
(54) Lee, J. S.; You, K. H.; Park, C. B. *Adv. Mater.* **2012**, *24*, 1084−1088.
(55) Li, D.; Muller, M. B.; Gilje, S.; Kaner, R. B.; Wallace, G. G. *Nat. Nanotechnol.* **2008**, *3*, 101−105.
(56) Szabo, T.; Tombacz, E.; Illes, E.; Dekany, I. *Carbon* **2006**, *44*, 537−545.
(57) Lin, G.; Zheng, J.; Xu, R. *J. Phys. Chem. C* **2008**, *112*, 7363−7370.
(58) Ai, Z.; Ho, W.; Lee, S. *J. Phys. Chem. C* **2011**, *115*, 25330−25337.
(59) Akhavan, O.; Choobtashani, M.; Ghaderi, E. *J. Phys. Chem. C* **2012**, *116*, 9653−9659.
(60) Chen, P.; Xiao, T.-Y.; Li, H.-H.; Yang, J.-J.; Wang, Z.; Yao, H.-B.; Yu, S.-H. *ACS Nano* **2011**, *6*, 712−719.
(61) Du, J.; Lai, X.; Yang, N.; Zhai, J.; Kisailus, D.; Su, F.; Wang, D.; Jiang, L. *ACS Nano* **2010**, *5*, 590−596.
(62) Hayashi, H.; Lightcap, I. V.; Tsujimoto, M.; Takano, M.; Umeyama, T.; Kamat, P. V.; Imahori, H. *J. Am. Chem. Soc.* **2011**, *133*, 7684−7687.
(63) Jiang, B.; Tian, C.; Pan, Q.; Jiang, Z.; Wang, J.-Q.; Yan, W.; Fu, H. *J. Phys. Chem. C* **2011**, *115*, 23718−23725.
(64) Luo, Q.-P.; Yu, X.-Y.; Lei, B.-X.; Chen, H.-Y.; Kuang, D.-B.; Su, C.-Y. *J. Phys. Chem. C* **2012**, *116*, 8111−8117.
(65) Mukherji, A.; Seger, B.; Lu, G. Q.; Wang, L. *ACS Nano* **2011**, *5*, 3483−3492.
(66) Ng, Y. H.; Iwase, A.; Kudo, A.; Amal, R. *J. Phys. Chem. Lett.* **2010**, *1*, 2607−2612.
(67) Williams, G.; Kamat, P. V. *Langmuir* **2009**, *25*, 13869−13873.
(68) Williams, G.; Seger, B.; Kamat, P. V. *ACS Nano* **2008**, *2*, 1487−1491.
(69) Calizo, I.; Balandin, A. A.; Bao, W.; Miao, F.; Lau, C. N. *Nano Lett.* **2007**, *7*, 2645−2649.
(70) Ferrari, A. C.; Meyer, J. C.; Scardaci, V.; Casiraghi, C.; Lazzeri, M.; Mauri, F.; Piscanec, S.; Jiang, D.; Novoselov, K. S.; Roth, S.; Geim, A. K. *Phys. Rev. Lett.* **2006**, *97*, 187401.
(71) Kim, K. S.; Zhao, Y.; Jang, H.; Lee, S. Y.; Kim, J. M.; Kim, K. S.; Ahn, J.-H.; Kim, P.; Choi, J.-Y.; Hong, B. H. *Nature* **2009**, *457*, 706−710.
(72) Kudin, K. N.; Ozbas, B.; Schniepp, H. C.; Prud'homme, R. K.; Aksay, I. A.; Car, R. *Nano Lett.* **2007**, *8*, 36−41.
(73) Chiu, C.-Y.; Chung, P.-J.; Lao, K.-U.; Liao, C.-W.; Huang, M. H. *J. Phys. Chem. C* **2012**, *116*, 23757−23763.
(74) Zhang, N.; Liu, S.; Fu, X.; Xu, Y.-J. *J. Phys. Chem. C* **2011**, *115*, 9136−9145.
(75) He, B.-L.; Dong, B.; Li, H.-L. *Electrochem. Commun.* **2007**, *9*, 425−430.
(76) Dai, K.; Dawson, G.; Yang, S.; Chen, Z.; Lu, L. *Chem. Eng. J.* **2012**, *191*, 571−578.
(77) Fu, H.; Xu, T.; Zhu, S.; Zhu, Y. *Environ. Sci. Technol.* **2008**, *42*, 8064−8069.
(78) Ma, L.-L.; Sun, H.-Z.; Zhang, Y.-G.; Lin, Y.-L.; Li, J.-L.; Wang, E.-k.; Yu, Y.; Tan, M.; Wang, J.-B. *Nanotechnology* **2008**, *19*, 115709.
(79) Moulijn, J. A.; van Diepen, A. E.; Kapteijn, F. *Appl. Catal., A* **2001**, *212*, 3−16.
(80) Pan, X.; Zhang, N.; Fu, X.; Xu, Y.-J. *Appl. Catal., A* **2013**, *453*, 181−187.
(81) Zhang, H.; Zhu, Y. *J. Phys. Chem. C* **2010**, *114*, 5822−5826.
(82) Zhang, H.; Zong, R.; Zhu, Y. *J. Phys. Chem. C* **2009**, *113*, 4605−4611.
(83) Zhang, L.; Cheng, H.; Zong, R.; Zhu, Y. *J. Phys. Chem. C* **2009**, *113*, 2368−2374.
(84) Bao, N.; Shen, L.; Takata, T.; Domen, K. *Chem. Mater.* **2007**, *20*, 110−117.
(85) Meissner, D.; Benndorf, C.; Memming, R. *Appl. Surf. Sci.* **1987**, *27*, 423−436.
(86) Akhavan, O.; Abdolahad, M.; Esfandiar, A.; Mohatashamifar, M. *J. Phys. Chem. C* **2010**, *114*, 12955−12959.
(87) Li, Z.; Zhang, W.; Luo, Y.; Yang, J.; Hou, J. G. *J. Am. Chem. Soc.* **2009**, *131*, 6320−6321.
(88) Ferry, J. L.; Glaze, W. H. *Langmuir* **1998**, *14*, 3551−3555.
(89) Gao, E.; Wang, W.; Shang, M.; Xu, J. *Phys. Chem. Chem. Phys.* **2011**, *13*, 2887−2893.
(90) Zhang, L. L.; Xiong, Z.; Zhao, X. S. *ACS Nano* **2010**, *4*, 7030−7036.